The changing nature of the active site of Cu-Zn-Zr catalysts for the CO_2 hydrogenation reaction to methanol

G. Bonura [a], M. Cordaro [b], C. Cannilla [a], F. Arena [b], F. Frusteri [a,*]

[a] CNR-ITAE, Institute for Advanced Energy Technologies "Nicola Giordano", Via S. Lucia sopra Contesse, 5, 98126 Messina, Italy
[b] Dept. Electronic Engineering,Industrial Chemistry & Engineering, University of Messina, V.le F. Stagno D'Alcontres 31, 98166 Messina, Italy

ARTICLE INFO

ABSTRACT

The effects of the most largely employed preparation methods (i.e., coprecipitation with sodium bicarbonate, complexation with citric acid, gel-oxalate coprecipitation) on the structure and catalytic behaviour of Cu-Zn-Zr systems for methanol synthesis from hydrogenation of carbon dioxide have been studied. The characterization data of the dried, calcined and reduced catalysts showed that the physico-chemical properties can be controlled by varying composition and preparation method. The catalyst obtained by the gel-coprecipitation procedure showed the highest catalytic activity in the T_R range 453–513 K, 3.0 MPa and 10,000 h^{-1}, due to a superior functionality in the CO_2 and H_2 activation. An adequate balance between metal and oxide surface sites, in correspondence of a well defined particle size, was proposed to be crucial to design active and selective catalysts for such reaction. The good performance of the gel-oxalate coprecipitated catalyst was confirmed by an endurance test ($\approx$200 h), in which a constant and remarkable methanol space–time-yield value of 1200 g kg$_{cat}^{-1}$ h^{-1} at $\approx$10% CO_2 conversion was obtained (T_R, 513 K; P_R, 3.0 MPa).

1. Introduction

The new technologies based on CO_2 capture and storage have recently received much attention, since the reduction of greenhouse emissions represents the main challenging issue on the climate change [1,2]. Although the efforts to develop new and more efficient adsorbents capable of capturing the atmospheric CO_2, alternative routes aimed at recycling carbon dioxide for the production of new chemicals or fuels, like methanol and dimethyl ether, appear more interesting and sustainable [3,4]. In particular, using CO_2 in place of CO for methanol synthesis would represent a decisive technological breakthrough with a remarkable improvement of the overall process economics [5–7].

As an alternative to Cu-Zn-Al catalysts, conventionally used for methanol synthesis from syngas [8–15], many authors have found that Cu-Zn-Zr catalysts are particularly effective for methanol synthesis too, especially in CO_2 hydrogenation reaction [16–31].

Notwithstanding nature of active sites and reaction pathways of methanol formation from CO_x–H_2 mixtures still remain matter of debate [32–36], to improve activity, selectivity or lifetime of such novel systems, several unconventional preparation routes have been adopted [17–23,25,27,28,37], mainly addressing either the copper surface area and dispersion [25,37] or the extent of metal-carrier oxide(s) interaction [17–20,22,28] or both of them [21,23,27] as crucial factors affecting the catalytic behaviour.

Among the preparation methods so far applied to confer textural, structural and surface properties suitable to obtain a good catalytic performance, the coprecipitation of salt precursors by sodium carbonate or bicarbonate in aqueous medium certainly is one of the most largely used [16–20,22–26,29–31]. The main reason of such a choice is based on the fact that the coprecipitation ensures a very good mixing of the various precursors during the solid formation step [23–26]. So, the very fine texture of the oxide particles, the sintering of which would be hindered by the release of great amounts of CO_2 from (hydroxy)carbonate decomposition during the calcination step, allows to obtain catalysts characterized by a large development of surface exposure [23].

It is also known that the citrate method provides solids with high surface areas, at relatively low calcination temperatures [25,27,37]. The peculiarity of the method consists in the initial formation of a homogeneous gel (containing the metal precursors) by complexing dissolved nitrate salts with citric acid.

Moreover, as reported by Ma and coworkers [28], $Cu/ZnO/ZrO_2$ catalysts prepared by oxalate coprecipitation method, in presence of ethanol (instead of water) as the solvent, exhibit fine and uniformly distributed catalyst particles, so also resulting in a high catalytic activity for methanol synthesis from CO_2 hydrogenation.

* Corresponding author. Tel.: +39090624233.
E-mail address: francesco.frusteri@itae.cnr.it (F. Frusteri).

The present study is focused to assess both the efficiency of the synthesis methodologies considered as the most promising in literature and the optimal catalyst composition of Cu–Zn–Zr systems, with the aim to improve their catalytic pattern in the CO_2 hydrogenation reaction to methanol.

2. Experimental

2.1. Catalyst preparation

Three Cu-Zn-Zr catalysts, with same atomic composition, were prepared according to the following methods.

Coprecipitation by $NaHCO_3$ (CB). The nitrates precursors of Cu, Zn and Zr were solubilized in H_2O and co-precipitated by adding $NaHCO_3$, at 353 K, under vigorous stirring and ultrasonic irradiation. The precipitate was repeatedly washed to remove Na^+ ions and then it was dried at 383 K for 16 h and finally calcined at 623 K for 4 h.

Complexation by citric acid (CT). The nitrates precursors of Cu, Zn, Zr were solubilized in H_2O and slowly added to a 1 M solution of citric acid. An intense blue color complex was formed. Then, the solvent was evaporated at low pressure, so obtaining a blue spongy solid. After drying at 383 K for 16 h, the solid was calcined at 623 K for 4 h.

Gel oxalate coprecipitation (OX). The precursors (nitrates of Cu, Zn, Zr) were solubilized in ethanol and coprecipitated by oxalic acid at room temperature under vigorous stirring. The precipitate was dried at 383 K for 16 h and then calcined at 623 K for 4 h.

2.2. Catalysts characterization

X-ray fluorescence (XRF). The analytical composition of catalysts was determined by X-ray fluorescence analysis, using a Bruker AXS-S4 Explorer spectrometer, equipped with a rhodium X-ray source (Rh anode and 75 μm Be-window), a LiF 220 crystal analyzer and a 0.12° divergence collimator. Samples were analyzed at the solid state, taking into account the emission value of Cu–$K_{\alpha 1}$, Zn–$K_{\alpha 1}$ and Zr–$K_{\alpha 1}$ transitions.

Surface area (SA) and pore volume (PV). The textural properties of catalysts were determined from nitrogen adsorption/desorption isotherms at −196 °C, using a Sorptomatic 1900 Instrument gas adsorption device. The isotherms were elaborated according to the BET method for surface area calculation, while Barrett–Joyner–Halenda (BJH) method was used for pore size distribution (PSD).

Scanning electron microscopy (SEM). SEM analysis was made by using a Philips XL-30-FEG microscope with an accelerating voltage of 5 kV. Specimens were prepared by gold sputtering of catalyst samples deposited as powders on aluminum pin flat stubs.

Thermo-gravimetry and differential scanning calorimetry (TG-DSC). Thermal analysis in the range of 293–1093 K was performed by using a Netzsch Simultaneous Thermal Analysis Instrument STA409C analyzer. The measurements were carried out in air with a heating rate of 10 K min^{-1}.

X-ray diffraction (XRD). Powdered samples were analyzed in the 2θ range 30–65° using a Philips X-Pert diffractometer, operating with Ni β-filtered Cu Kα radiation (λ = 1.5406 Å) at 40 kV and 30 mA and a scan step of 0.05° s^{-1}.

Temperature programmed reduction (TPR). The measurements of reducibility were performed in hydrogen atmosphere using a linear quartz micro-reactor (i.d. 4 mm) fed with a 5 vol.% H_2/Ar at the flow rate of 30 stp mL min^{-1}. The experiments were carried out in the range 273–1073 K with a heating rate of 20 K min^{-1}. The hydrogen consumption was monitored by a TCD, previously calibrated by loading the reactor with a known amount of CuO. TPR data resulted

very reproducible both in the maximum position (±3 K) and extent of H_2 consumption (±3%).

N_2O titration measurements. Copper surface area (MSA) and dispersion (D_{Cu}) values were obtained by "single-pulse" N_2O-titration measurements at 363 K [23]. Before measurements the samples were reduced at 573 K in flowing H_2 (100 stp mL min^{-1}) for 1 h, then "flushed" at 583 K in nitrogen carrier flow (15 min) and further cooled down at 363 K. MSA and D_{Cu} values were calculated assuming a Cu:N_2O = 2:1 titration stoichiometry and a surface atomic density of 1.46×10^{19} Cu$_{at}$/m^2, respectively [23], while, assuming a spherical shape, the Cu average particle size (d_{Cu}) was obtained from the conventional formula [23]:

$$d_{Cu}(nm) = \frac{104}{D_{Cu}}(\%).$$

2.3. Catalyst testing

The catalytic activity was investigated in a continuous fixed-bed stainless steel reactor (internal diameter, 4 mm; length, 200 mm) at 3.0 MPa. Standard experiments were carried out by using 0.125 g of catalyst (40–70 mesh), diluted with granular SiC (0.125 g), under a reactant flow rate of 1.4 stp L/h (CO_2/H_2/N_2 = 3/9/1) in the temperature range 453–513 K, prior to each test, the catalyst was reduced in situ at 573 K for 1 h with pure hydrogen flow at atmospheric pressure. The reaction stream was analyzed by a GC equipped with a two-column system connected to a flame ionized detector (FID) and thermal conductivity detector (TCD) respectively.

Activity-selectivity data were obtained at steady-state conditions after 1.5 h of time on stream, at reaction temperature. CO_2 conversion values (X_{CO_2}) were calculated by both internal standard (a) and mass-balance (b) methods,

$$X_{CO_2} = 1 - \left[\left(\frac{CO_{2,out}}{CO_{2,in}} \right) \times \left(\frac{N_{2,in}}{N_{2,out}} \right) \right] \tag{a}$$

and

$$X_{CO_2} = \frac{CO_{2,out}}{(\Sigma P_i + CO_{2,out})}, \tag{b}$$

with product selectivity data (S_{P_i}) obtained from standard equations:

$$S_{P_i} = \frac{P_i}{(1 - CO_{2,out})} \tag{a'}$$

and

$$S_{P_i} = \frac{P_i}{\Sigma_{P_i}} \tag{b'}$$

where P_i stands for the concentration of a specific i product (i.e., CH_3OH, CO).

Each data set was obtained, with an accuracy of ±3%, from an average of three independent measurements.

Equilibrium data were calculated by solving the system of non linear equations obtained from the equilibrium constants, K_{P_1} and K_{P_2}:

$$K_{P_1} = \frac{p_{CH_3OH,eq} \times p_{H_2O,eq}}{P_{CO_2,eq} \times p_{H_2,eq}^3} \tag{a}$$

$$K_{P_2} = \frac{p_{CO,eq} \times p_{H_2O,eq}}{p_{CO_2,eq} \times p_{H_2,eq}} \tag{b}$$

where $p_{CO_2} = (0.23 - x - y) \times P^0$; $p_{H_2} = (0.69 - 3x - y) \times P^0$; $p_{CH_3OH} = x \times P^0$; $p_{CO} = y \times P^0$; $p_{H_2O} = (x + y) \times P^0$ and P^0 is the experimental pressure (MPa).

Table 1
Physico-chemical properties of the prepared catalysts.

Catalyst	Composition (wt.%)[a]			SA$_{BET}$ (m^2 g^{-1})		PV (cm^3 g^{-1})		APD (Å)[b]	
	CuO	ZnO	ZrO$_2$	Calcined	Reduced	Calcined	Reduced	Calcined	Reduced
C6Z3Z1-CB	57.1	28.1	14.8	158	121	0.237	0.194	60	64
C6Z3Z1-CT	56.4	27.7	15.9	132	108	0.195	0.162	59	60
C6Z3Z1-OX	56.8	27.7	15.5	162	145	0.235	0.228	58	63

[a] From XRF measurements.
[b] Average pore diameter (APD, 4 × PV/SA).

3. Results and discussion

3.1. Catalyst characterization

A composition of 60/30/10 was chosen for the preparation of the Cu–Zn–Zr samples, considering that ternary Cu–ZnO based catalysts with similar composition exhibited high activity in the CO$_2$-to-methanol hydrogenation reaction [10,11,25,31,38]. Differently from coprecipitation with NaHCO$_3$, which represents the most widely used technique to prepare Cu-based systems [32–34], the complexation with citric acid or coprecipitation with oxalic acid allowed to obtain catalysts free of alkaline contamination.

The analytical composition as well as the corresponding textural properties of the prepared catalysts, before and after activation under H$_2$ atmosphere, are summarized in Table 1. Notwithstanding a high CuO loading (56–57 wt.%), irrespective of the preparation method all the samples present high surface area (132–162 m^2 g^{-1}),

confirming that the concentration of ZnO is sufficient to effectively act as a "spacer" [32,33], favouring so a good exposure of total surface area. For all the samples, after H$_2$ reduction at 573 K, the surface area decreases, as well as the pore volume, in consequence of copper particles sintering upon the exposure to a reducing environment. However, on the C6Z3Z1-OX sample, these phenomena appear rather limited (ΔSA ≈ 10%; ΔPV ≈ 3%), likely because the gel-like precipitate formed during preparation should ensure a better molecular-scale mixing of the precursors, enhancing so the resistance to the growth of metal crystallites upon reduction [10,26,33,39]. In spite of higher surface area and pore volume of C6Z3Z1-CB and C6Z3Z1-OX coprecipitated catalysts, the average pore diameter results to be similar (APD ≈ 60 Å) to that of the C6Z3Z1-CT sample, remaining substantially unchanged even after reduction.

Fig. 1 shows the PSD, calculated according to the BJH method, and the morphology of the sample evaluated by SEM
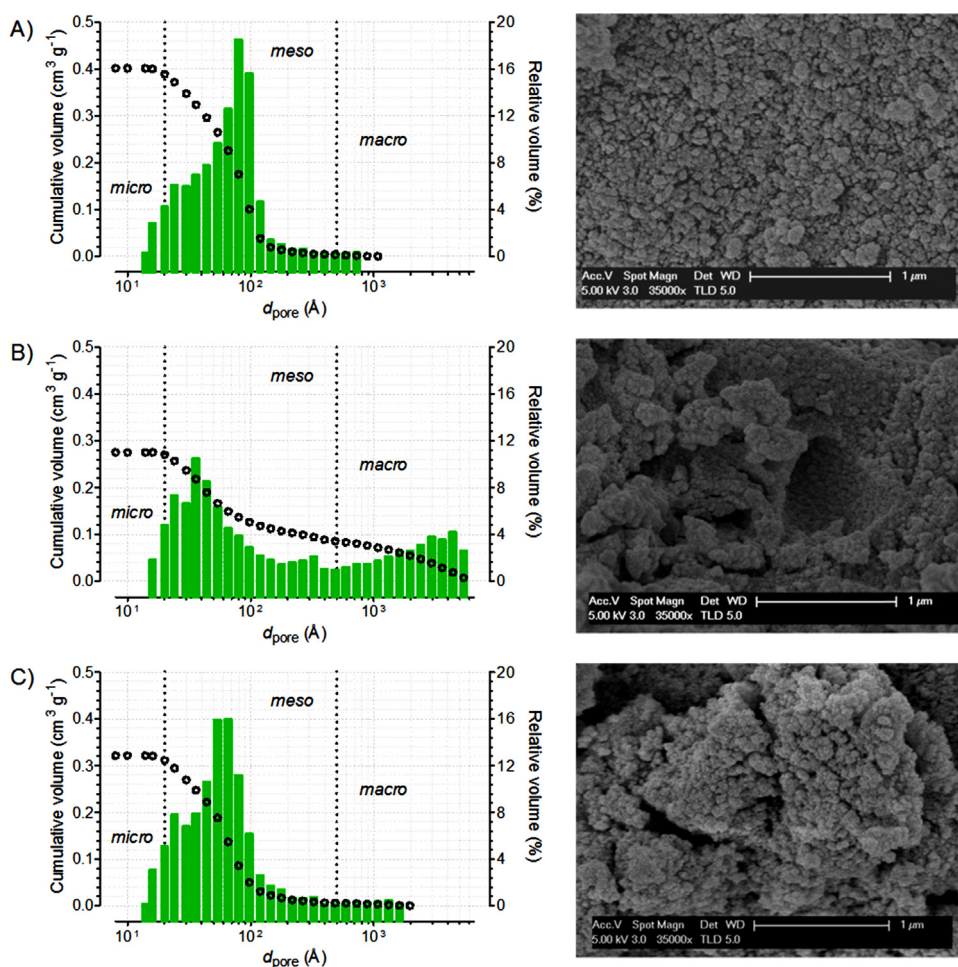

Fig. 1. Pore size distribution (left) and SEM micrographs (right) of the prepared catalysts: (A) C6Z3Z1-CB; (B) C6Z3Z1-CT; (C) C6Z3Z1-OX.

measurements. It is possible to observe that both coprecipitated catalysts (Figs. 1A and C) essentially present mesopores of diameter comprised between 25 and 115 Å, while the C6Z3Z1-CT sample is characterized by a bimodal PSD, exhibiting a not negligible macro-porosity (2000–5000 Å), despite a minor cumulative pore volume (0.195 cm^3 g^{-1}). SEM image of Fig. 1B well shows the existence of large cavities over the catalyst texture, likely originated by the citrate decomposition. A homogeneous distribution of spherical particles was obtained when sodium bicarbonate was used as the precipitating agent (Fig. 1A), while more aggregated particles were found during coprecipitation in presence of oxalic acid (Fig. 1C).

Thermal analysis, performed to investigate the decomposition behaviour of the dried precursors are shown in Fig. 2. While the TG-DSC pattern of the dried C6Z3Z1-CB catalyst (Fig. 2A) exhibits a moderate mass loss (<30%) ascribable to (hydroxy)carbonate decomposition, the mass loss observed for the C6Z3Z1-CT and C6Z3Z1-OX samples (Figs. 2B and C), prepared starting from organic precursors (i.e., citric and oxalic acid, respectively), is consider-ably higher (>60%). Such a mass loss is, fundamentally, due to the evolution of physisorbed water (T < 393 K) along with incipi-ent dehydroxylation (473–563 K) and oxidation of organic residues (563–623 K). On the basis of this result, a calcination temperature of 623 K was adopted to ensure complete decomposition of catalyst precursor(s) and minimize sintering phenomena.

XRD measurements, performed to obtain information on the crystalline phases present on the samples reduced under H$_2$ atmo-sphere at 573 K for 1 h, are collected in Fig. 3. For all the samples, the main peaks at 2θ values of 43.2 and 50.4, which are indexed to <1 1 1> and <2 0 0> diffraction planes respectively, are consistent with the JCPDS 01-089-2838 and associated to metallic copper. The other diffraction peaks matched the standard data for a hexagonal wurtzite ZnO (JCPDS 36-1451). Since all the XRD patterns exhibit identical 2θ angles, it can be concluded that, upon reduction, the samples are completely reduced to metallic Cu without any detec-tion of Cu$_2$O or CuO phases, also showing that the experimental variables during preparation did not alter significantly the main crystalline phases of the samples.

TPR profiles, shown in Fig. 4, display for all the samples a main H$_2$ consumption peak centered at 531–554 K (see also Table 2) and shouldered on the left side of the maximum. Such a peak is diagnostic of a quantitative reduction of CuO to metallic Cu below 573 K, whereas the slight differences both in the onset reduc-tion ($T_{o,red}$) and the maxima temperature (T_M) can be explained on the basis of the extent of copper-oxide(s) interaction, affected by the different preparation procedure used. The baseline drift observed at 573–973 K, with a poorly resolved temperature max-imum (830–890 K), was associated with an ongoing reduction of the ZnO promoter [23]. Although the total H$_2$ consumption (9.2–10.4 mmol g^{-1}) does not allow to stress significant differences in terms of reducibility promoted by solid state interactions, for all the samples the ratio between the amount of H$_2$ consumed and the amount of reducible copper oxide in the temperature range 293–593 K was higher (1.07–1.18) than that expected on the basis of stoichiometry (H$_2$/Cu = 1.00). This surplus of H$_2$ consumption is generally associated to ZnO and copper crystallites capable to store large amounts of hydrogen both on surface and in subsurface regions [39,40].

Regarding N$_2$O chemisorption data (see Table 2), the metal surface area (MSA) was found to vary between 18 (C6Z3Z1-CT) and 28 m$^2_{Cu}$ g^{-1} (C6Z3Z1-OX), accounting for copper dispersion of 6.3 and 9.5% respectively, whereas the copper particle diameter measures 110 Å for C6Z3Z1-OX, 140 Å for C6Z3Z1-CB and 165 Å for C6Z3Z1-CT.

Fig. 5 shows that the copper surface area of the different cata-lysts linearly increases with the BET surface area. Nevertheless, a wider copper dispersion also accounts for a decreasing of the onset
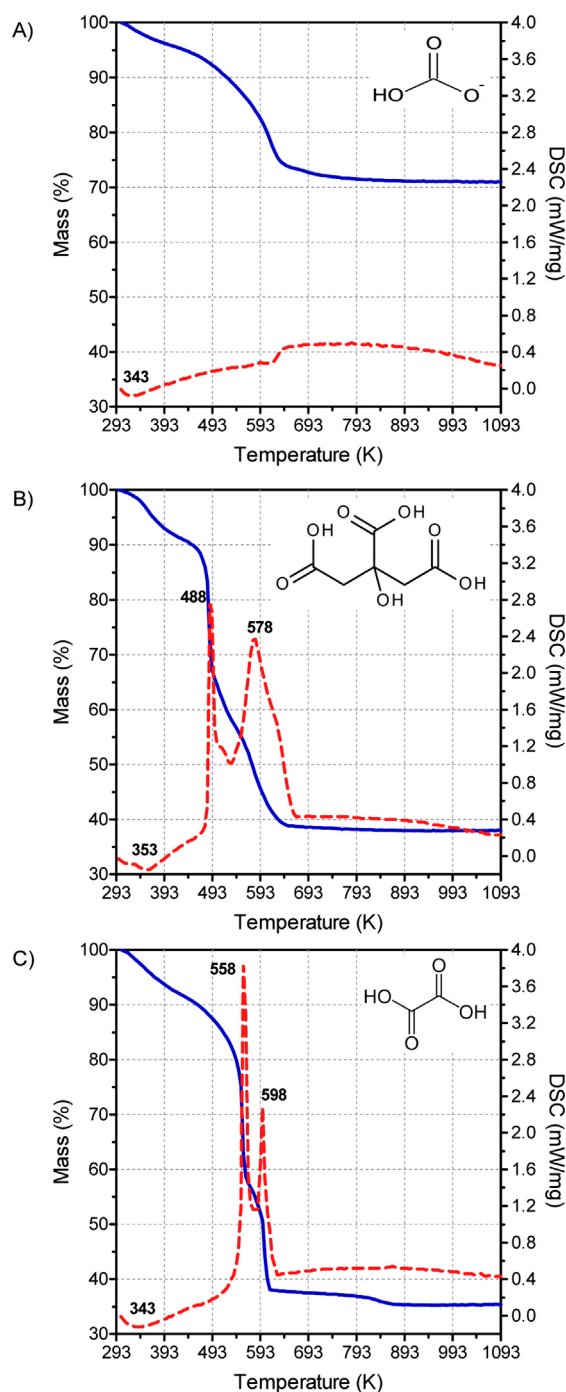

Fig. 2. TG and DSC profiles of the "dried" catalysts: (A) C6Z3Z1-CB; (B) C6Z3Z1-CT; (C) C6Z3Z1-OX.

temperature reduction ($T_{o,red}$), as the result of a faster reactivity of smaller (d_{Cu} < 140 nm) Cu^{2+} surface species. On the contrary, a minor copper dispersion is diagnostic of a stronger interaction of large CuO particles with ZnO that definitely causes a shift of $T_{o,red}$ towards higher temperature.

3.2. Catalytic behaviour

Activity data of Cu–Zn–Zr catalysts in the CO$_2$ hydrogena-tion reaction (T_R = 453–513 K; P_R = 3.0 MPa; GHSV = 10,000 h^{-1}) are reported in Table 3, in terms of CO$_2$ conversion (X_{CO_2}), selectiv-ity to CH$_3$OH (S_{CH_3OH}) and CO (S_{CO}) and yield of CH$_3$OH (Y_{CH_3OH}).

Table 2
Surface properties from H_2-TPR and N_2O chemisorption measurements.

Catalyst	$T_{o,red}$ (K)	T_M (K)	H_2 consumption ($mmol_{tot}\,g^{-1}$)	H_2/Cu[a]	MSA ($m^2{}_{Cu}\,g^{-1}$)[b]	D_{Cu} (%)[b]	d_{Cu} (Å)[b]
C6Z3Z1-CB	406	543	10.1	1.12	23	7.4	140
C6Z3Z1-CT	408	554	10.4	1.18	18	6.3	165
C6Z3Z1-OX	393	531	9.2	1.07	28	9.5	110

[a] From H_2-TPR: T range 293–593 K.
[b] From N_2O chemisorption measurements.

Table 3
Catalytic performance of the CuZnZr systems.[a]

Catalyst	T_R (K)	X_{CO_2} (%)	S_{CH_3OH} (%)	S_{CO} (%)	Y_{CH_3OH} (%)	E_a ($kJ\,mol^{-1}$)
C6Z3Z1-CB	453	2.9	92.4	7.7	2.6	57 ± 2
	473	5.9	75.2	24.8	4.4	
	493	11.1	61.3	38.7	6.8	
	513	16.0	48.7	51.3	7.8	
C6Z3Z1-CT	453	1.9	100.0	0.0	1.9	63 ± 3
	473	4.0	86.2	13.8	3.4	
	493	7.6	71.0	29.0	5.4	
	513	12.5	51.8	48.2	6.5	
C6Z3Z1-OX	453	3.6	89.1	11.0	3.2	52 ± 2
	473	7.0	73.5	26.3	5.1	
	493	14.0	64.1	35.7	9.0	
	513	18.0	51.2	48.6	9.2	

[a] Reaction conditions: P_R = 3.0 MPa; GHSV = 10,000 h^{-1}.

Methanol and carbon monoxide were the only carbon-containing products found.

In the temperature range investigated, the C6Z3Z1-CB sample features X_{CO_2} values raising from 2.9 to 16.0%, while S_{CH_3OH} correspondingly decreases from 92.4 to 48.7%, accounting for Y_{CH_3OH} comprised between 2.6 and 7.8%. Moreover, the C6Z3Z1-CT system, prepared by citrate method, exhibits considerably low conversion and selectivity levels, to which correspond a maximum Y_{CH_3OH} of 6.5% at high temperature. On the other hand, the coprecipitation by oxalic acid determines a positive effect on the activity pattern of the C6Z3Z1-OX system, mostly in terms of X_{CO_2}. This implies higher X_{CO_2} values at any investigated temperature (3.6–18.0%), with a maximum Y_{CH_3OH} of 9.2% at 513 K. On the basis of such results, the catalytic performance of the studied systems can be summarized in the following activity scale, referred to the methanol yield achieved in the range of 453–513 K:

$$C6Z3Z1 - OX > C6Z3Z1 - CB \gg C6Z3Z1 - CT$$

As reported in Table 3, this activity scale accounts for a relatively higher apparent energy values of the C6Z3Z1-CT catalyst prepared by citrate method (E_a, 63 kJ/mol) in comparison to C6Z3Z1-CB (57 kJ/mol) and C6Z3Z1-OX (52 kJ/mol) coprecipitated catalysts. This matches the finding that the coprecipitation method enables an easier reactivity of the adsorbed CO_2, owing to the presence of smaller particles that favour a larger development of
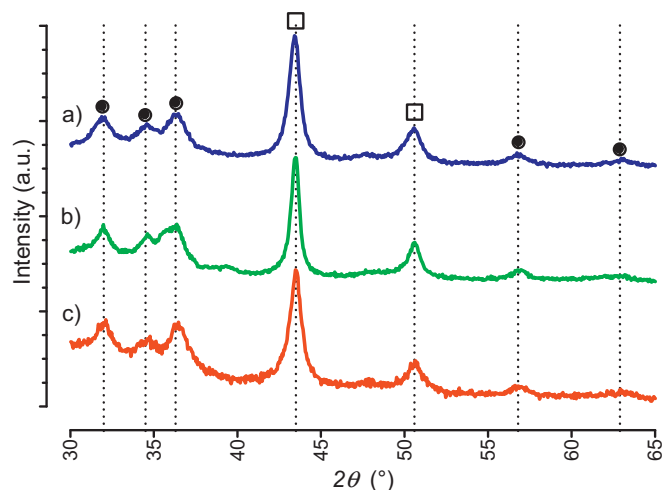

Fig. 3. XRD of the reduced samples (□ Cu^0; ● ZnO): (a) C6Z3Z1-CB; (b) C6Z3Z1-CT; (c) C6Z3Z1-OX.
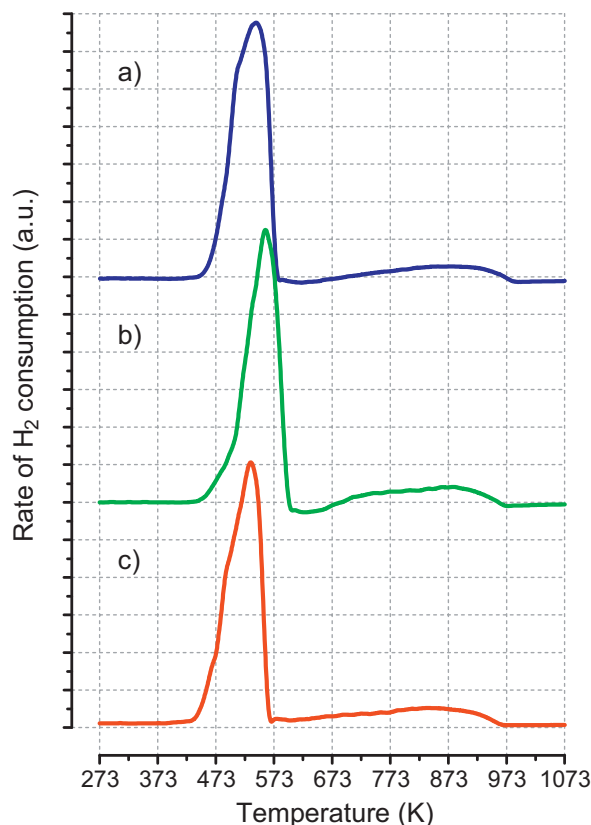

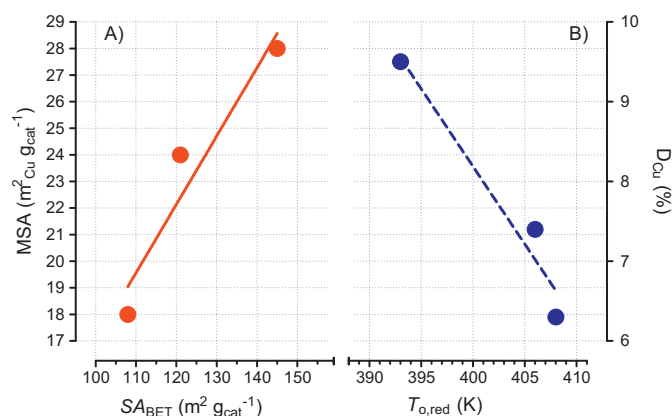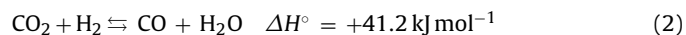**Fig. 4.** H_2-TPR profiles: (a) C6Z3Z1-CB; (b) C6Z3Z1-CT; (c) C6Z3Z1-OX.

Fig. 5. (A) Relationship between MSA and SA_{BET}. (B) Influence of copper dispersion on $T_{o,red}$.

metal-oxide(s) interfacial area, where the reaction intermediates (formate/dioxo-methylene/methoxy species) form before to be further hydrogenated to methanol [16,22,32].

In Fig. 6A the selectivity as a function of carbon dioxide conversion, at different temperature, is shown. Independently of the catalyst used, it is clear that high methanol selectivity is obtainable at low CO_2 conversions. In fact, as well known, the CO_2 hydrogenation process takes place according to two competitive reactions: (1) methanol synthesis and (2) reverse water–gas shift (RWGS). The equilibrium of such reactions can be described as follows:

$$CO_2 + 3H_2 \leftrightarrows CH_3OH + H_2O \quad \Delta H° = -49.5 \, kJ \, mol^{-1} \tag{1}$$

$$CO_2 + H_2 \leftrightarrows CO + H_2O \quad \Delta H° = +41.2 \, kJ \, mol^{-1} \tag{2}$$

Obviously, by increasing the reaction temperature, the endothermic RWGS reaction results to be favoured.

The temperature dependence of the methanol production rate (STY) over catalysts prepared by different methods is shown in Fig. 6B. As a reference, equilibrium data for the temperature range

investigated are also reported. For all the samples, a rising methanol productivity was observed in the range 453–513 K. In particular, a higher productivity was reached by the C6Z3Z1-OX sample, with STY values of 108 and 305 $g_{CH_3OH}kg_{cat}^{-1} h^{-1}$ at 453 and 513 K, respectively. Instead, the citrate-complexed catalyst showed low activity for the methanol synthesis reaction, attaining a maximum of $216 g_{CH_3OH}kg_{cat}^{-1} h^{-1}$ 216 $g_{CH3OH} kg_{cat}^{-1} h^{-1}$ at 513 K.

At a first glance, such a catalytic behaviour was directly ascribed to the differences in the copper surface area existing among the prepared systems (see Table 2). However, as also confirmed by other authors [22,25,32,33,35,36,40], this is only one factor to be considered among others which can control the catalyst activity, like the formation of a very intimate contact between metallic copper and oxide carriers [35], the stabilisation of low-valence state copper species ($Cu^{\delta+}$) onto oxygen surface vacancies [32], a change in the morphology of the metallic sites [39].

Considering the interesting behaviour of the C6Z3Z1-OX sample prepared by gel oxalate coprecipitation, in order to investigate the effect of composition on the catalytic performance, two new catalysts characterized by a lower copper loading (46 at.% in C4Z2Z4 and 33 at.% in C3Z3Z3, respectively) were also synthesized by the same method (see Table 4). As reported, the progressive decreasing of copper content (which results in a higher cumulative concentration of zinc and zirconium), accounts for a decreasing in the shrinkage of surface area upon reduction ($\Delta SA = 17 \, m^2 \, g^{-1}$ for C6Z3Z1-OX, $5 \, m^2 \, g^{-1}$ for C4Z2Z4-OX and $3 \, m^2 \, g^{-1}$ for C3Z3Z3-OX), as the result of a less marked tendency to the metal sintering, inhibited by a higher massive content of Zn and Zr oxides in the two new samples. Moreover, a decrease of MSA (from 28 to $17 m_{Cu}^2 g^{-1}$) with the copper loading corresponds to a systematic increase of D_{Cu} (from 9.5 to 12.0%), also mirroring the presence of copper particles characterized by smaller d_{Cu} ($110 \rightarrow 85$ Å). Then, determining the texture of the final catalysts, it was expected that a change in the metal-to-oxide surface ratio ($R_{MSA/OSA}$, where OSA = SA − MSA) could reflect a different CO_2-hydrogenation functionality of the catalyst. By comparing the results in terms of STY (see Fig. 7), it has been seen that, at any investigated reaction temperature, the C6Z3Z1-OX sample, characterized by the highest $R_{MSA/OSA}$ (0.24 vs. 0.18 of C4Z2Z4-OX
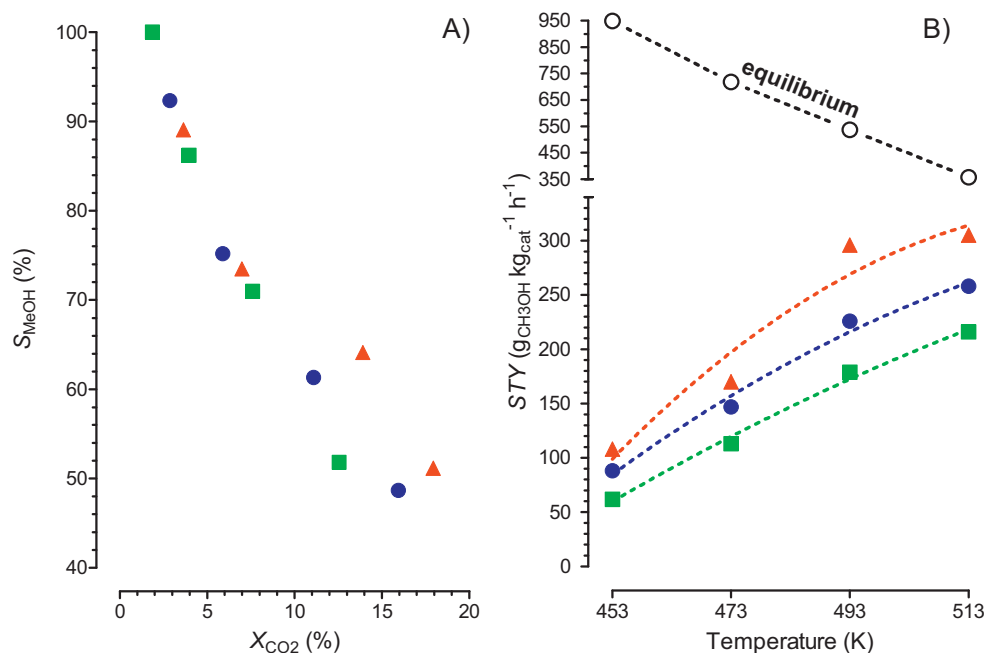

Fig. 6. (A) Methanol selectivity as a function of CO_2 conversion and (B) STY of the prepared catalysts in the T_R range 453–513 K (P_R = 3.0 MPa; GHSV = 10,000 h^{-1}). Catalysts: ● C6Z3Z1-CB; ■ C6Z3Z1-CT; ▲ C6Z3Z1-OX.

Table 4
Properties of the gel oxalate coprecipitated catalysts.

Catalyst	Composition (at.%)[a]			SA_{BET} ($m^2 g^{-1}$)		MSA ($m^2_{Cu} g^{-1}$)[b]	D_{Cu} (%)[b]	d_{Cu} (Å)[b]	$R_{MSA/OSA}$[c]
	Cu	Zn	Zr	Calc	Red				
C6Z3Z1-OX	60	29	11	162	145	28	9.5	110	0.24
C4Z2Z4-OX	46	15	39	159	154	24	10.8	95	0.18
C3Z3Z3-OX	33	33	34	161	158	17	12.0	85	0.12

[a] From XRF measurements.
[b] From N_2O chemisorption measurements.
[c] $R_{MSA/OSA}$, metal-to-oxide surface ratio; $OSA = SA - MSA$.

and 0.12 of C3Z3Z3-OX), still exhibited the best performance, since the methanol productivity regularly increased with $R_{MSA/OSA}$, again addressing the need for a large MSA as the key to obtain high specific activity.

In order to confirm such findings, considering the dual-site nature of the reaction pathway (H_2 activation on Cu^0 sites and CO_2 activation in the neighbouring of the interface oxide(s) sites) [17,18,22,32,33], the activity of the catalysts was compared on the basis of turnover frequencies, which were calculated either as molecules of methanol formed per second on Cu^0 surface site (TOF_{MSA}) or as molecules of carbon dioxide reacted per second on oxides surface sites (TOF_{OSA}). As shown in Fig. 8, the intrinsic activity of the catalysts does not remain constant with the increasing of the copper dispersion, but it follows two specular exponential-like trends, so that, on the C3Z3Z3-OX sample, the highest frequency of methanol production on Cu^0 sites (that reveals an apparent higher activity of smaller Cu^0 particles) is offset by the lowest frequency of CO_2 conversion on oxide sites. This clearly demonstrates that the performance of the Cu–Zn–Zr catalysts cannot be merely considered as a function of the availability of H_2 or CO_2 activated on surface, but rather the occurrence of structural and chemical effects

related to different reactivity and surface adsorption sites of the Cu–Zn–Zr systems needs to be taken into account too.

Therefore, since also the copper particle size could significantly affect the catalytic behaviour, the methanol selectivity obtained on the different catalysts was compared at constant CO_2 conversion levels too (see Fig. 9). At X_{CO_2} as low as 3%, a higher methanol selectivity ($S_{CH_3OH} > 90\%$) is achieved either in presence of small ($d_{Cu} = 85–95$ Å) or large Cu^0 crystallites ($d_{Cu} = 140–165$ Å). Likely, under a prevailing reducing environment and a low concentration of water formed, smaller Cu^0 crystallites (more easily reducible and well dispersed in the neighbouring of the surface oxides) as well as larger Cu^0 crystallites result to be highly selective to methanol. Instead, at higher CO_2 conversion ($X_{CO_2} = 6 - 9\%$), the formation of water should be responsible for a partial oxidation of the metallic sites [22], inhibiting the formation of CH_3OH mainly on small (on which the oxidation rate should be enhanced [17,18]) or large (that can remain in the metallic form [41]) copper particles. This confirms that, in the CO_2 hydrogenation reaction, not only a metal functionality is required, but an efficient interaction among the metal (Cu^0)
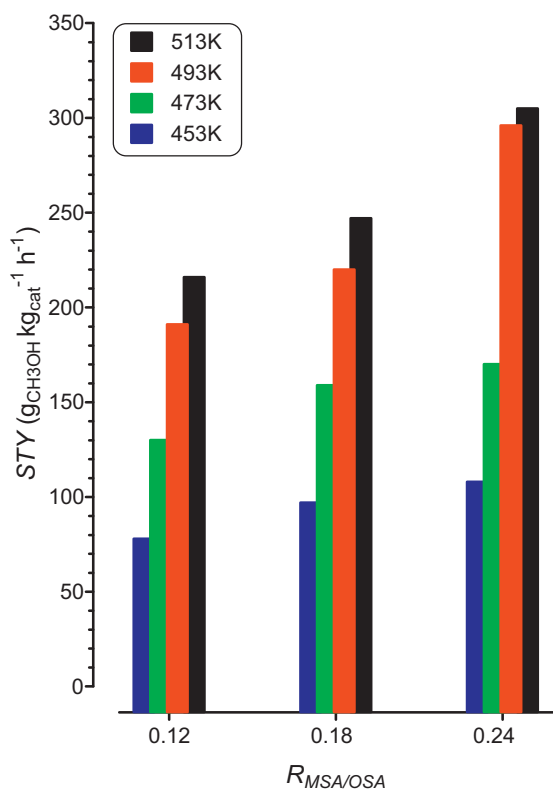

Fig. 7. Influence of the metal-to-oxide(s) ratio ($R_{MSA/OSA}$) on the catalytic productivity ($P_R = 3.0$ MPa; GHSV = 10,000 h^{-1}).
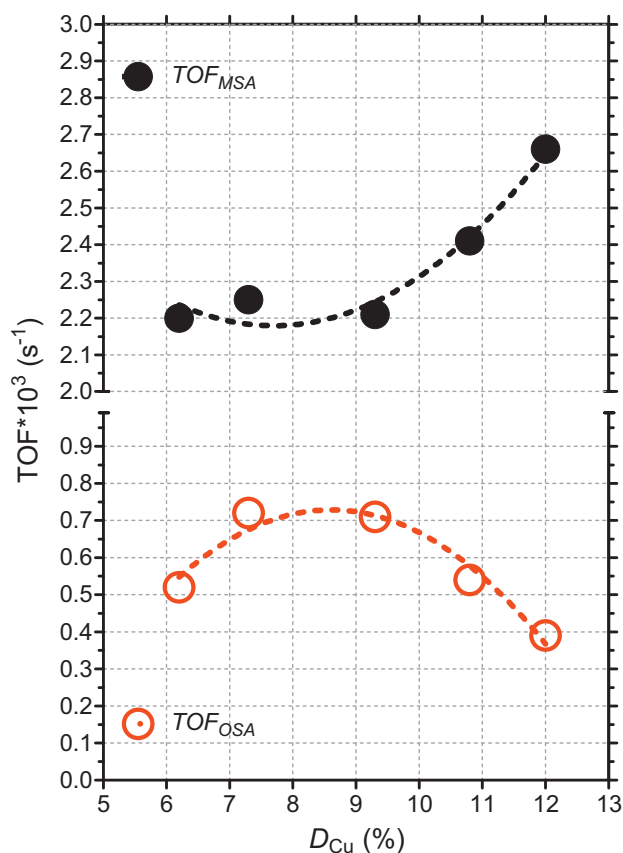

Fig. 8. Influence of copper dispersion (D_{Cu}) on the rate of methanol formation per Cu^0 site per second (TOF_{MSA}) and on the rate of CO_2 conversion per oxide site per second (TOF_{OSA}) ($T_R = 473$ K; $P_R = 3.0$ MPa; GHSV = 10,000 h^{-1}).
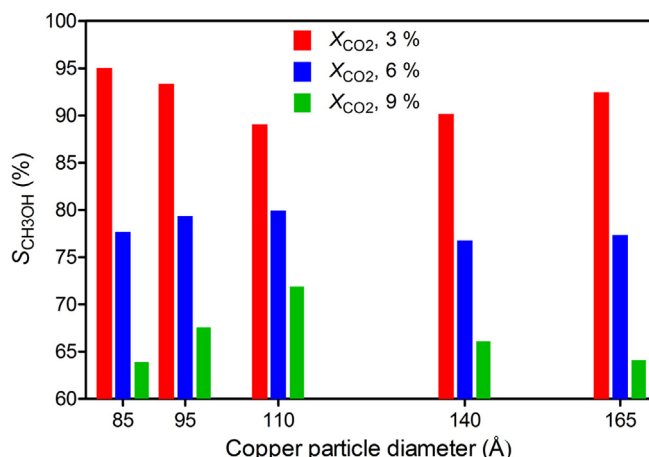
Fig. 9. Methanol selectivity as a function of copper particle diameter at constant conversion ($P_R = 3.0$ MPa; GHSV = 10,000 h^{-1}).

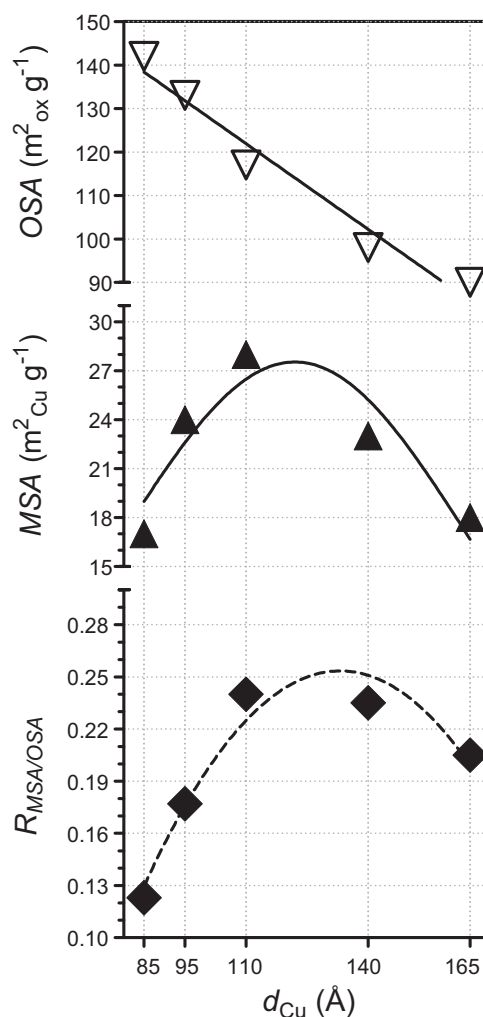Fig. 10. Relationships of MSA (metal surface area), OSA (oxide surface area) and $R_{MSA/OSA}$ (metal-to-oxide surface ratio) with the copper dispersion (D_{Cu}) for the investigated catalysts.

and the oxide sites (ZnO and ZrO$_2$) is also necessary to ensure high methanol selectivity [28]. Indeed, such interaction is effectively realized in presence of particles characterized by a well defined size, so favouring the methanol formation even in a more oxidative environment [22,33,37]. Evidently, the generation of such active sites is favoured when a suitable extent of MSA/OSA interfacial area does exist [22], being promoted both by solid state interactions, typical of the preparation procedure adopted, and by the chemical composition. These considerations are supported by the results shown in Fig. 10, which reveal that the $R_{MSA/OSA}$ ratio changes with the copper particle size according to a volcano-shaped trend, in which the maximum availability of Cu^0 sites is obtained in correspondence of particles of 110 Å. On the whole, if from one hand the size of the particles can be controlled depending on the preparation method adopted, from the other hand a suitable distribution among metal and oxides sites (i.e., MSA/OSA ratio) is a crucial factor to get high methanol selectivity.

The space velocity is another important factor that could affect the methanol synthesis reaction. As shown in Fig. 11, by increasing the space velocity from 10,000 to 80,000 h^{-1}, the CO$_2$ conversion decreases from 18 to 9%, while methanol space-time yield increases from 305 to 1210 g$_{CH_3OH}$ kg$_{cat}^{-1}$ h^{-1}. Overall, as reported in Table 5, such productivity data for methanol production from CO$_2$ hydrogenation result among the highest so far experimentally determined for similar Cu-Zn-Zr catalysts, even in more favourable conditions [17–19,32]. Moreover, from Fig. 11, when the contact time is long enough (GHSV $\leq$ 55,000 h^{-1}), CO prevails on CH$_3$OH formation. On the contrary, by increasing the space velocity, methanol selectivity progressively increases at expense of carbon monoxide, until at a space velocity as high as 80,000 h^{-1} the

relative CH$_3$OH/CO selectivity is close to 1. Basically, if both CH$_3$OH and CO were exclusively formed from the main reactions (1)–(2), the CH$_3$OH/CO selectivity ratio should remain unchanged with the space velocity. Instead, the change of the selectivity ratio with space velocity suggests that the potential occurrence of side reactions must be also considered. In such a case, a possible secondary reaction is represented by the methanol decomposition (3):
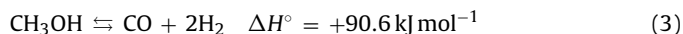
$$CH_3OH \leftrightarrows CO + 2H_2 \quad \Delta H^\circ = +90.6 \text{ kJ mol}^{-1} \tag{3}$$

Table 5
Productivity data of Cu-Zn-Zr catalysts.

| Catalyst composition (at.%)	T_R (K)	P_R (MPa)	GHSV (NL g$_{cat}^{-1}$ h^{-1})	STY (g$_{CH_3OH}$ kg$_{cat}^{-1}$ h^{-1})	Ref.
Cu(57)Zn(17)Zr(26)	513	3.0	15,000	375	[16]
Cu(51)Zn(17)Zr(32)	513	3.0	8800–55,000	300–740	[17,18]
Cu(51)Zn(17)Zr(32)	513	5.0	8800–55,000	510–1200	[17,18]
Cu(49)Zn(19)Zr(33)	513	3.0	8800	180	[19]
Cu(53)Zn(14)Zr(33)	513	3.0	4400	140	[23]
Cu(49)Zn(44)Zr(7)	523	3.0	2750[a]	60	[24]
Cu(70)Zn(24)Zr(6)	493	8.0	3300	170	[25]
Cu(45)Zn(45)Zr(10)	513	2.0	7800	160	[28]
Cu(60)Zn(25)Zr(15)	523	5.0	16,500	620	[30]
Cu(53)Zn(25)Zr(22)	473	0.9	4800	50	[31]
Cu(60)Zn(29)Zr(11)	513	3.0	10,000–80,000	305–1200	This paper

[a] Stirred tank reactor, mixing rate = 1000 rpm.
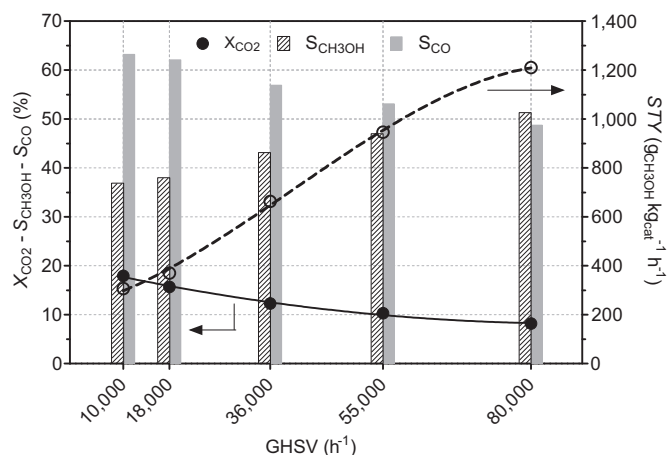
Fig. 11. Influence of the space velocity on conversion-selectivity data and methanol space–time yield. Catalyst: C6Z3Z1-OX ($T_R = 513$ K; $P_R = 3.0$ MPa).
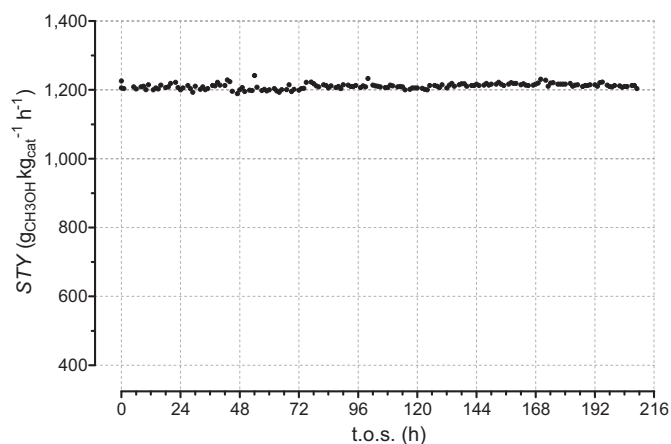

Fig. 12. Trend of methanol STY vs. time on stream. Catalyst: C6Z3Z1-OX ($T_R = 513$ K; $P_R = 3.0$ MPa; GHSV = 80,000 h^{-1}).

Since at low contact time the reactions proceed in an one-way direction, being depressed the reverse reactions, the simultaneous formation of CO and CH_3OH can be certainly explained on the basis of a parallel reaction pathway involving the CO_2 hydrogenation reaction. On the other hand, by lowering the space velocity, the increasing of CO selectivity in correspondence of the decreasing of CH_3OH selectivity clearly proofs that CO is not formed exclusively via RWGS reaction, but also the methanol decomposition reaction has a significant "weight" on the formation of carbon monoxide under the adopted experimental conditions.

Considering the interesting results obtained with the C6Z3Z1-OX gel-coprecipitated catalyst, an endurance test was carried out at 3.0 MPa, 513 K and space velocity of 80,000 h^{-1}. As shown in Fig. 12, the catalyst maintains a very high productivity of 1200g$_{CH_3OH}$kg$_{cat}$$^{-1}$h^{-1} for over 200 h, without any appreciable decreasing during time on stream, so demonstrating an excellent and stable catalytic performance under the reaction conditions investigated.

4. Conclusions

Three Cu-Zn-Zr catalysts for methanol synthesis from CO_2 hydrogenation were prepared by conventional sodium bicarbonate coprecipitation, complexation with citric acid and gel-oxalate coprecipitation method, respectively.

Irrespective of a high Cu loading (60 at.%), the preparation conditions significantly affect structure, surface properties and redox behaviour of the catalysts.

The catalyst prepared *via* the gel-oxalate coprecipitation method showed a superior functionality, attaining a specific productivity of 305g$_{CH_3OH}$kg$_{cat}$$^{-1}$h^{-1} at 513 K, 3.0 MPa and 10,000 h^{-1}.

The turnover frequency data revealed that the catalytic behaviour is not exclusively dependent on the availability of the surface oxides (mainly responsible for CO_2 activation) or metallic sites (mainly responsible for H_2 activation), but rather on the extent of the interfacial surface area, determined by a proper interaction between metal and oxide.

Experiments performed at high space velocity suggested that methanol is mainly formed from CO_2 rather than CO hydrogenation.

A remarkable space-time yield of 1200g$_{CH_3OH}$kg$_{cat}$$^{-1}$h^{-1}, constant for over 200 h, was obtained on the gel-oxalate coprecipitated catalyst, evidencing a very stable behaviour under the experimental conditions used.

References

[1] A.A. Olajire, Energy 35 (2010) 2610–2628.
[2] M. Aresta, in: M. Maroto-Valer (Ed.), Carbon Dioxide Capture and Storage, Woodhead Publishing Limited, Abington Hall, Granta Park, Cambridge, CB21 6AH, UK, 2009.
[3] G. Centi, E.A. Quadrelli, S. Perathoner, Energy Environ. Sci. 6 (2013) 1711–1731.
[4] G. Centi, S. Perathoner, Catal. Today 148 (2009) 191–205.
[5] G.A. Olah, Angew. Chem. Int. Ed. 52 (2013) 104–107.
[6] M. Peters, B. Köhler, W. Kuckshinrichs, W. Leitner, P. Markewitz, T.E. Müller, ChemSusChem 4 (2011) 1216–1240.
[7] C. Song, Catal. Today 115 (2006) 2–32.
[8] X. Zhang, L. Zhong, Q. Guo, H. Fan, H. Zheng, K. Xie, Fuel 89 (2010) 1348–1352.
[9] E. Kleymenov, J. Sa, J. Abu-Dahrieh, D. Rooney, J.A. van Bokhoven, E. Troussard, J. Szlachetko, O.V. Safonova, M. Nachtegaal, Catal. Sci. Technol. 2 (2012) 373–378.
[10] C. Baltes, S. Vukojević, F. Schüth, J. Catal. 258 (2008) 334–344.
[11] I. Kasatkin, P. Kurr, B. Kniep, A. Trunschke, R. Schlögl, Angew. Chem. 119 (2007) 7465–7468.
[12] Y.-L. Zhang, Q. Sun, J.-F. Deng, D. Wu, S.-Y. Chen, Appl. Catal. A 158 (1997) 105–120.
[13] G. Chinchen, P. Denny, J. Jennings, M. Spencer, K. Waugh, Appl. Catal. 36 (1988) 1–65.
[14] J.L. Li, T. Inui, Appl. Catal. A 139 (1996) 87–96.
[15] J.S. Lee, K.H. Lee, S.Y. Lee, Y.G. Kim, J. Catal. 144 (1993) 414–424.
[16] R. Ladera, F.J. Pérez-Alonso, J.M. González-Carballo, M. Ojeda, S. Rojas, J.L.G. Fierro, Appl. Catal. B (2013) 241–248.
[17] F. Arena, G. Mezzatesta, G. Zafarana, G. Trunfio, F. Frusteri, L. Spadaro, J. Catal. 300 (2013) 141–151.
[18] F. Arena, G. Mezzatesta, G. Zafarana, G. Trunfio, F. Frusteri, L. Spadaro, Catal. Today 210 (2013) 39–46.
[19] G. Bonura, F. Arena, G. Mezzatesta, C. Cannilla, L. Spadaro, F. Frusteri, Catal. Today 171 (2011) 251–256.
[20] F. Arena, G. Italiano, K. Barbera, G. Bonura, L. Spadaro, F. Frusteri, Catal. Today 143 (2009) 80–85.
[21] X. Guo, D. Mao, G. Lu, S. Wang, G. Wu, J. Catal. 271 (2010) 178–185.
[22] F. Arena, G. Italiano, K. Barbera, S. Bordiga, G. Bonura, L. Spadaro, F. Frusteri, Appl. Catal. A 350 (2008) 16–23.
[23] F. Arena, K. Barbera, G. Italiano, G. Bonura, L. Spadaro, F. Frusteri, J. Catal. 249 (2007) 185–194.
[24] R. Raudaskoski, M.V. Niemelä, R.L. Keiski, Top. Catal. 45 (2007) 57–60.
[25] J. Słoczyński, R. Grabowski, P. Olszewski, A. Kozłowska, J. Stoch, M. Lachowska, J. Skrzypek, Appl. Catal. A 310 (2006) 127–137.
[26] J. Słoczyński, R. Grabowski, A. Kozłowska, P. Olszewski, J. Stoch, J. Skrzypek, M. Lachowska, Appl. Catal. A 278 (2004) 11–23.
[27] J. Słoczyński, R. Grabowski, A. Kozłowska, P. Olszewski, M. Lachowska, J. Skrzypek, J. Stoch, Appl. Catal. A 249 (2003) 129–138.
[28] Y. Ma, Q. Sun, D. Wu, W.H. Fan, Y.L. Zhang, J.F. Deng, Appl. Catal. A 171 (1998) 45–55.

[29] M. Saito, T. Fujitani, I. Takahara, T. Watanabe, M. Takeuchi, Y. Kanai, K. Moriya, T. Kakumoto, Energy Convers. Manage. 36 (1995) 577–580.

[30] T. Fujitani, M. Saito, Y. Kanai, T. Kakumoto, T. Watanabe, J. Nakamura, T. Uchijima, Catal. Lett. 25 (1994) 271–276.

[31] Y. Nitta, O. Suwata, Y. Ikeda, Y. Okamoto, T. Imanaka, Catal. Lett. 26 (1994) 345–354.

[32] W. Wang, S. Wang, X. Ma, J. Gong, Chem. Soc. Rev. 40 (2011) 3703–3727.

[33] X.-M. Liu, G.Q. Lu, Z.-F. Yan, J. Beltramini, Ind. Eng. Chem. Res. 42 (2003) 6518–6530.

[34] V.E. Ostrovskii, Catal. Today 77 (2002) 141–160.

[35] I.A. Fisher, A.T. Bell, J. Catal. 172 (1997) 222–237.

[36] J. Nakamura, I. Nakamura, T. Uchijima, Y. Kanai, T. Watanabe, M. Saito, T. Fujitani, J. Catal. 160 (1996) 65–75.

[37] A. Karelovic, A. Bargipant, C. Fernández, P. Ruiz, Catal. Today 197 (2012) 109–118.

[38] P.J.A. Tijm, F.J. Waller, D.M. Brown, Appl. Catal. A 221 (2001) 275–282.

[39] S.-I. Fujita, S. Moribe, Y. Kanamori, M. Kakudate, N. Takezawa, Appl. Catal. A 207 (2001) 121–128.

[40] Ahouari, A. Soualah, A. Le Valant, L. Pinard, P. Magnoux, Y. Pouilloux, React. Kinet. Mech. Catal. 110 (2013) 131–145.

[41] T. Witoon, T. Permsirivanich, W. Donphai, A. Jaree, M. Chareonpanich, Fuel Process. Technol. 116 (2013) 72–78.